ACS APPLIED MATERIALS & INTERFACES

Research Article

www.acsami.org

Electronic Structure and Band Alignment at an Epitaxial Spinel/Perovskite Heterojunction

Liang Qiao,*[,†] Wei Li,[‡,§] Haiyan Xiao,[∥,⊥] Harry M. Meyer,[#] Xuelei Liang,[§] N. V. Nguyen,[‡] William J. Weber,[⊥] and Michael D. Biegalski*[,†]

[†]Center for Nanophase Materials Sciences and [#]Materials Science and Technology Division, Oak Ridge National Laboratory, Oak Ridge, Tennessee 37831, United States

[‡]Semiconductor and Dimensional Metrology Division, National Institute of Standards and Technology, Gaithersburg, Maryland 20899, United States

[∥]School of Physical Electronics, University of Electronic Science and Technology of China, Chengdu 610054, China

[⊥]Department of Materials Science and Engineering, University of Tennessee, Knoxville, Tennessee 37996, United States

[§]Key Laboratory for the Physics and Chemistry of Nanodevices and Department of Electronics, Peking University, Beijing 100871, China

Supporting Information

ABSTRACT: The electronic properties of solid−solid interfaces play critical roles in a variety of technological applications. Recent advances of film epitaxy and characterization techniques have demonstrated a wealth of exotic phenomena at interfaces of oxide materials, which are critically dependent on the alignment of their energy bands across the interface. Here we report a combined photoemission and electrical investigation of the electronic structures across a prototypical spinel/perovskite heterojunction. Energy-level band alignment at an epitaxial $Co_3O_4/SrTiO_3(001)$ heterointerface indicates a chemically abrupt, type I heterojunction without detectable band bending at both the film and substrate. The unexpected band alignment for this typical p-type semiconductor on $SrTiO_3$ is attributed to its intrinsic d−d interband excitation, which significantly narrows the fundamental band gap between the top of the valence band and the bottom of the conduction band. The formation of the type I heterojunction with a flat-band state results in a simultaneous confinement of both electrons and holes inside the Co_3O_4 layer, thus rendering the epitaxial $Co_3O_4/SrTiO_3(001)$ heterostructure to be a very promising material for high-efficiency luminescence and optoelectronic device applications.

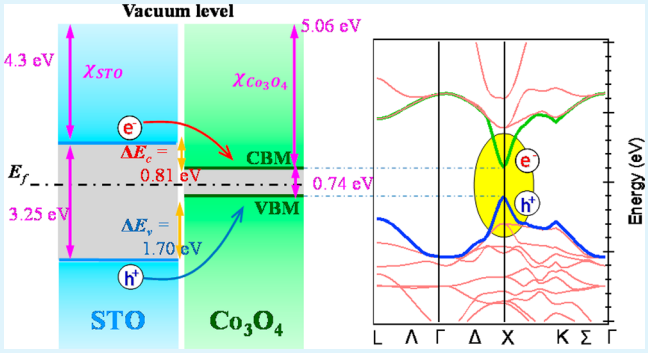

KEYWORDS: *spinel/perovskite heterojunction, electronic structure, band alignment, photoemission*

INTRODUCTION

Since first proposed by Keoemer et al. in 1954, heterojunctions composed of III−V and II−VI semiconductors have been the basis for the majority of solid-state devices.[1] In such devices, the energy-level band-alignment-induced valence- and conduction-band discontinuities, or band offsets, between semiconductors are critical parameters in determining their physical properties, such as electron−hole pair separation, confinement, and transport behavior. Depending on the respective sizes of the energy gaps of the constituted materials, there are mainly two types of heterojunctions, straddling (type I) and staggered (type II). Successful engineering of these properties in semiconductors has been shown to be very important for information technology and energy applications.

As a comparison, our knowledge of band-alignment phenomena regarding analogous interfacial systems involving oxide materials is quite limited. For example, band offsets at rutile and anatase TiO_2 interfaces have been greatly debated over last 2 decades.[2] Recently, oxide materials, especially epitaxial oxide thin films, have been demonstrated to exhibit surprisingly enormous multifunctional properties, some of which are not possible in conventional semiconductors, e.g., colossal magnetoresistance and magnetoelectric coupling.[3−5] Critical scientific issues exist, ranging from adhesion of dissimilar oxide materials to interfacial electronic states, ionic and electronic reconstruction, and its effect on electron/spin/magnetic transport and scattering, for example, recent exciting discoveries and the resulting debates on the two-dimensional electron gas at perovskite/perovskite[6,7] and spinel/perovskite heterojunctions.[8] Therefore, unveiling the interfacial electronic

Received: June 8, 2014
Accepted: July 21, 2014
Published: July 21, 2014

structure and energy-level band alignment and determining the correct band-offset values for oxide heterojunctions are of vital importance for a deeper understanding and better control of these intriguing properties for the advancement of oxide electronics and photovolatics.

Spinel Co_3O_4 is a very classic transitional-metal oxide that has been investigated for more than a half-century because of its unusual electronic, magnetic, optical, and chemical properties and important industrial interests, e.g., lithium battery, solar adsorption, gas sensing, and surface catalysis.[9−11] In contrast to their interesting bulk material properties and wide technological applications, fundamental knowledge regarding electronic fine structure, interband excitation, and band alignment at energy level remains much less understood and contradictions in the assignment of electronic transitions still remain for Co_3O_4.[12−15] Furthermore, $SrTiO_3$ (STO) is a very important oxide substrate for the growth of high quality oxide thin films and heterostructures.[16,17] Epitaxial integration of Co_3O_4 with STO and understanding the band alignment, energy offset, carrier confinement, and interfacial electronic structure of this particular heterojunction are important for the realization of highly efficient cobalt-based oxide devices.

In this paper, we report a combined photoemission spectroscopy and electrical-based energy-level band-alignment determination for epitaxial Co_3O_4/STO(001) heterojunction, at which unexpected, but potentially useful band-offset behavior is observed. Contrary to the general idea that intimate contact of a p-type semiconductor on top of an n-type one will result in a type II heterojunction, the band alignment at the Co_3O_4/STO(001) heterointerface is actually a type I heterojunction. We demonstrate that this result is due to intrinsic d−d interband excitations of Co_3O_4, which significantly narrows the fundamental band gap between the top of the valence band (VB) and the bottom of the conduction band (CB). Basic electronic parameters, e.g., the work function and electron affinity, for Co_3O_4 are also obtained based on Anderson's rule. Both the film and substrate exhibit a flat-band state without any detectable band bending at the heterojunction. These electronic features result in a simultaneous quantum confinement of both electrons and holes inside the Co_3O_4 layer, thus rendering the Co_3O_4/STO(001) heterojunction to be a very promising material for high-efficiency luminescence and optoelectronic device applications.

RESULTS AND DISCUSSION

Figure 1 shows a typical out-of-plane X-ray diffraction (XRD) $2\theta-\omega$ scan for a 100 nm Co_3O_4 film grown on STO(001). It is seen that only the (002) and (004) peaks are observed, suggesting that the Co_3O_4 film grows into a high (001) orientation without the presence of any detectable secondary phases or impurities. The absence of odd (h00) peaks, e.g., (001) and (003), is due to the extinction rule for a spinel lattice. In-plane lattice matching is measured through φ scans for both Co_3O_4 and STO on (202) reflections, as shown in the left inset. The overlap of the four Bragg peaks for the film and substrate reveals the expected cube-on-cube growth with the epitaxial relationship Co_3O_4(100) [001]||STO(100) [001].

Strain is known to have a large impact on some semiconductor band offsets, e.g., the Si/Ge system and piezoelectric GaN/AlN/InN.[18,19] However, because of the relative large lattice misfit between the film and substrate, $(^1/_2 a_{film} - a_{sub})/a_{sub} \sim 3.46\%$, the Co_3O_4 film grown on STO is completely relaxed.[20−22] For these strain levels, the Matthews−

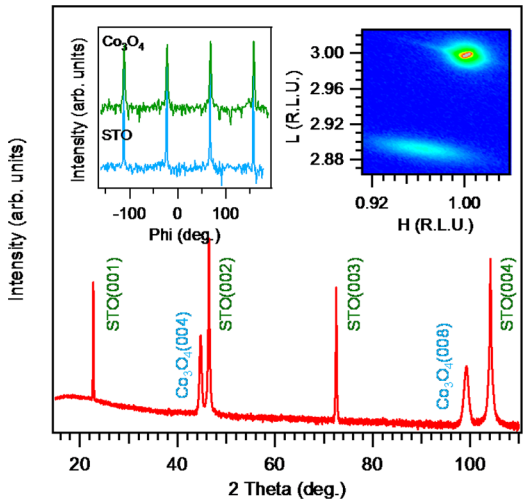

Figure 1. Typical XRD symmetric $2\theta-\omega$ scan for 100 nm epitaxial Co_3O_4/STO indicating the spinel structure of Co_3O_4. The left inset shows the XRD (202) φ scan for both the film and substrate, indicating a cube-on-cube epitaxial relationship, and the right inset is the (103) RSM, showing that the film is relaxed but maintains epitaxy with STO.

Blakeslee elastic model predicts a critical thickness of approximately 1 unit cell.[23] This is also consistent with the reflective high-energy electron diffraction (RHEED) pattern observations, where no shift of the RHEED diffraction pattern occurs after the initial film growth. The right inset shows the (103) reciprocal space map (RSM) of the same Co_3O_4/STO film. The displacement of the momentum transfer along H between the film and substrate indicates a different in-plane lattice spacing, resulting in the relaxed structure of the epitaxial Co_3O_4 film. These structural characterizations demonstrate the formation of a relaxed epitaxial Co_3O_4/STO heterostructure.

In photoionization processes, the band offset of a heterojunction with intimate contact of dissimilar materials is a measure of the energy differences of their valence-band maximum (VBM) or conduction-band minimum (CBM) between the two materials after alignment of their chemical potential, or Fermi level. Therefore, the binding energies of some specific core-level peaks and VBM for both the individual materials and their heterojunction are needed. Here we choose bulk STO(001) and the 100 nm Co_3O_4 film as reference surfaces for pure materials. Two core-level peaks from STO (Sr $3d_{5/2}$ and Ti $2p_{3/2}$) and Co_3O_4 (Co 3p and Co $2p_{3/2}$) are chosen to calculate the band offset. Thus, four distinct combinations of core levels, with each pair consisting of one STO peak and one Co_3O_4 peak, are used to check consistency.[24,25] VB offsets (ΔE_v) are calculated based on the energy differences of the core-level peaks with respect to their VBM for the thick film, bulk substrate, and thin heterojunction, as developed by Kraut et al.[26−28] in the following expressions:

$$\Delta E_v^{Co\,2p-Sr} = (E_{Co\,2p} - E_v)_{Co_3O_4} - (E_{Sr\,3d} - E_v)_{STO} + (E_{Sr\,3d} - E_{Co\,2p})_{HJ} \quad (1)$$

$$\Delta E_v^{Co\,3p-Sr} = (E_{Co\,3p} - E_v)_{Co_3O_4} - (E_{Sr\,3d} - E_v)_{STO} + (E_{Sr\,3d} - E_{Co\,3p})_{HJ} \quad (2)$$

dx.doi.org/10.1021/am5036219 | ACS Appl. Mater. Interfaces 2014, 6, 14338−14344

$$\Delta E_v^{\mathrm{Co\,2p-Ti}} = (E_{\mathrm{Co\,2p}} - E_v)_{\mathrm{Co_3O_4}} - (E_{\mathrm{Ti\,2p}} - E_v)_{\mathrm{STO}} + (E_{\mathrm{Ti\,2p}} - E_{\mathrm{Co\,2p}})_{\mathrm{HJ}} \quad (3)$$

$$\Delta E_v^{\mathrm{Co\,3p-Ti}} = (E_{\mathrm{Co\,3p}} - E_v)_{\mathrm{Co_3O_4}} - (E_{\mathrm{Ti\,2p}} - E_v)_{\mathrm{STO}} + (E_{\mathrm{Ti\,2p}} - E_{\mathrm{Co\,3p}})_{\mathrm{HJ}} \quad (4)$$

where the first two terms in eqs 1−4, labeled Co_3O_4 and STO, are determined from the thick Co_3O_4 film and the STO substrate, respectively, and the last term, labeled HJ, is measured from the 2 nm Co_3O_4/STO heterojunction. Figure 2 shows high-energy-resolution X-ray photoelectron spectroscopy (XPS) survey spectra from −5 to 145 eV for Co_3O_4, STO, and Co_3O_4/STO, which cover the core levels of both Sr 3d and Co 3p as well as their VBs, as shown in insets. All of these spectra were collected during the same run (without breaking vacuum) to minimize the systematic uncertainty caused by surface charge compensation. The VBM values for the reference surfaces are determined through linear extrapolation of the leading edge of the VB region to the extended baseline of the VB spectra in order to account for the instrumental broadening. This linear method has already been proven to consistently yield correct VBMs for semiconductors with an accuracy of about ±0.1 eV.[29] The obtained VBM values for reference Co_3O_4 and bulk STO are 0.01(4) and 4.01(4) eV, respectively. The energy positions of the core-level peaks are obtained by fitting the spectra with a Voigt line shape. The Co 2p, Ti 2p, and Sr 3d spectra are well-resolved spin−orbital split pairs (see the Supporting Information, SI), and the energies of the more intense higher angular momentum peaks were used in the band-offset calculation, i.e., Co $2p_{3/2}$, Ti $2p_{3/2}$, and Sr $3d_{5/2}$. The Co 3p peaks in both thick and thin films exhibit a single peak and are slightly asymmetric because of the presence of a shakeup excitation in the higher-energy shoulder. This is typical in 3d metal oxide, and the main peak at lower binding energy is used to calculate the peak position.[7] Particularly, the Ti 3s peak (see SI) partially overlaps with the Co 3p peak because of the relatively small binding energy differences (~1 eV), and this overlap becomes weaker when the film is thicker. Therefore, for a film thinner than 2 nm, the contribution of Ti 3s was also modeled through the use of a reference STO substrate with the appropriate photoelectron attenuation based on our previous method.[24] The energy differences between the core levels and VBMs for reference Co_3O_4 are 779.68(4) and 60.78(4) for Co $2p_{3/2}$ and Co 3p, respectively, and those values for STO are 455.97(4) and 130.67(4) for Ti $2p_{3/2}$ and Sr $3d_{5/2}$, respectively. These data match the reported values for Co_3O_4[9] and STO[24] in the literature. We then measure the energy differences of each core-level pair in the thin heterojunction for the four orbitals. Thus, the calculated valence-band orbitals (VBOs) are $\Delta E_v^{\mathrm{Co\,2p-Sr}}$ = 1.74(6) eV, $\Delta E_v^{\mathrm{Co\,3p-Sr}}$ = 1.64(6) eV, $\Delta E_v^{\mathrm{Co\,2p-Ti}}$ = 1.76(8) eV, and $\Delta E_v^{\mathrm{Co\,3p-Ti}}$ = 1.66(8) eV, respectively. The arithmetic mean and standard deviation of these give a ΔE_v value of 1.70 ± 0.08 eV. Further analysis on heterojunctions with 1 and 3 nm Co_3O_4 yields similar ΔE_v values of 1.72 ± 0.08 and 1.65 ± 0.04 eV, respectively. This indicates that when spinel Co_3O_4 is aligned with perovskite STO in energy space, their respective band-edge positions do not change as a function of the film thickness, resulting in a constant band-offset condition.

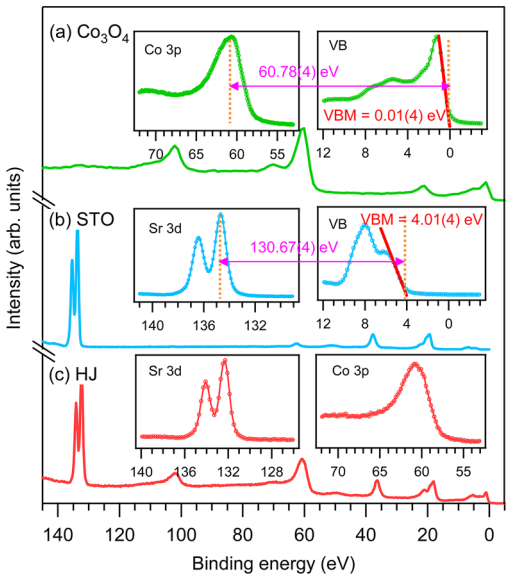

Figure 2. High-energy-resolution XPS spectra for a Co_3O_4 thick film (a), bulk STO (b), and thin Co_3O_4(2 nm)/STO heterojunction (c) from −5 to 145 eV binding energy. The insets of each figure show the corresponding Co 3p, Sr $3d_{5/2}$, and VB spectra for all references. VBM values for Co_3O_4 and STO are determined by linearly extrapolating the leading edge of the VB region to the extended baseline of the VB spectra, as indicated by the solid lines in the inset figures.

To confirm that there are no artifacts in the data, which may complicate the band offsets, the VB spectra of the Co_3O_4/STO heterojunctions were also simulated by shifting and summing the appropriately weighted high-resolution survey spectra for thick reference spectra for Co_3O_4 and STO based on inelastic photoelectron attenuation models.[24,25] These spectra were shifted in energy and scaled so that the Sr 3d and Co 3p binding energies and peak areas match those of the heterojunction. The energy shifting is required to eliminate the differences between the core-level binding energies for the reference spectra and the heterojunction to cancel the surface potential accumulation induced by X-ray beam irradiation, while the intensity weighting is required to account for the inelastic attenuation of substrate photoelectrons by the overlaying epitaxial film. ΔE_v for the heterojunction is then calculated as the difference between the VBM for the two reference surfaces relative to the Fermi level. As expected, in this case, the direct superposition of the intensity-weighted VB spectra for the two clean surfaces mimics that of the actual heterojunction. The results of these simulations are shown in Figure 3a for Co_3O_4/STO heterojunctions with different thicknesses of the Co_3O_4 layer from 1 to 3 nm. The agreements between the simulated and experimental heterojunction spectra are excellent with respect to both the positions and relative intensities for all features regardless of the Co_3O_4 film thickness (see the dash-dotted lines in the figure), confirming the self-consistency and accuracy of the method. Moreover, the high accuracy of the agreements also demonstrates that the interface of the Co_3O_4/STO heterojunction is chemically abrupt without the formation of any detectable interfacial states.

We determine the CB offset (ΔE_c) using the following equation:

$$\Delta E_c = \Delta E_v + (E_g^{\mathrm{Co_3O_4}} - E_g^{\mathrm{STO}}) \quad (5)$$

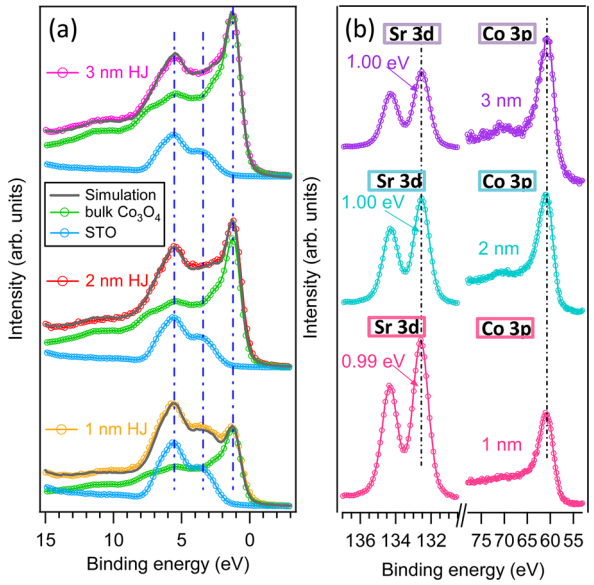

Figure 3. (a) Comparison of the VB spectra for the reference Co_3O_4 thick film, bulk STO, and thin heterojunction with 1 nm (orange), 2 nm (red), and 3 nm (magenta) Co_3O_4 coverage, as well as a simulation of the VB for each thin heterojunction. The matching of experimental spectra and simulation of the VB indicates that the interface of the Co_3O_4/STO heterojunction is chemically abrupt without the presence of any interfacial states. (b) Sr 3d and Co 3p core-level peaks as a function of the Co_3O_4 layer thickness. The absence of peak shifting for these two core levels suggests no band bending at the heterojunction.

Note that ΔE_c is critically dependent on the size of the band gaps for both the film and substrate. Electronic transitions in Co_3O_4 had been previously investigated by optical absorption as well as ellipsometry, and multiple interband transitions had been demonstrated.[12−15] The typical band gap for Co_3O_4 reported in the literature is 1.6−2.2 eV.[12,30,31] We have recently demonstrated that while the ∼2.0 eV transition is the stronger optical excitation because of its larger oscillator strength of the p−d-type transition, it is not the fundamental band gap of this material.[32] Instead, the lower-energy transition at ∼0.74 eV should be considered as the fundamental band gap for Co_3O_4, as evidenced by our optical absorption and photoluminescence spectroscopy as well as photoluminescence excitation mapping.[32] Because both the top of the VB and the bottom of the CB are primarily of Co 3d features, this energy gap is considered a d−d-type interband transition. Using eq 5, the common E_g^{STO} of ∼3.25 eV for STO,[33,34] $E_g^{Co_3O_4}$ of 0.74 eV, and ΔE_v of 1.70 eV, ΔE_c is determined to be −0.81 ± 0.08 eV. The negative value of the obtained ΔE_c indicates that the CBM is lower in the epitaxial Co_3O_4 film than in the STO substrate. On the basis of the obtained ΔE_c value, some basic electronic parameters of Co_3O_4, i.e., the electron affinity (χ) and work function (ϕ), can be estimated using Anderson's electron affinity rule.[35] It is reported for undoped STO that the work function is 4.6 eV and the energy difference of the Fermi level versus the VBM ($E_f - E_v$) is 2.9 eV, respectively.[36] Taking the E_g value of 3.25 eV for STO into account, the electron affinity for STO is calculated to be $\chi = \phi + (E_f - E_v) - E_g = 4.25$ eV. Thus, the electron affinity for Co_3O_4 is obtained by $\chi_{Co_3O_4} = \chi_{STO} - CBO = 5.06$ eV. This value is larger than 3.5 eV reported by Miura et al. by electrical measurement.[37] The inconsistency is ascribed to the relatively large error bar of their original data (±0.5 eV) and the overestimation of the fundamental band gap for Co_3O_4. It is also important to note that Co_3O_4 is a p-type semiconductor; thus, the Fermi level should be fairly close to the VBM. When a midgap position of the Fermi energy is assumed, the work function for Co_3O_4 is ∼5.43 eV, which is consistent with the estimated second-electron cutoff energy determined by ultraviolet photoelectron spectroscopy.[38−40]

The CB alignment is further confirmed by an electrical-based internal photoemission (IPE) spectroscopy method, which has been shown to be a robust technique to determine electronic band alignment in semiconductor heterostructures. When the transition of carriers is induced from one material to another through optical excitation, IPE can directly measure the band offsets at the interfaces.[41,42] It is seen in Figure 4 that, under

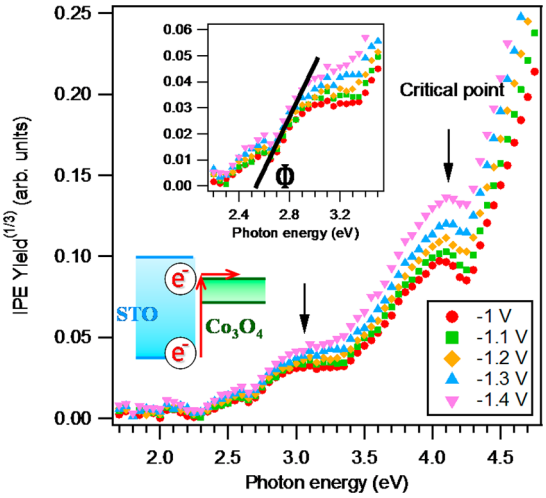

Figure 4. Constructed energy-level band alignment at the Co_3O_4/STO(001) heterojunction. The complete overlap of both the VB and CB of the Co_3O_4 film with respect to the STO substrate indicates a type I heterojunction. The inset is a magnified IPE to show how the barrier height is extracted.

negative bias, the obtained photoelectric quantum yield shows several inflections as a function of the incidence photon energy. The peaks at 3.0 and 4.1 eV (black arrows) are critical points for bulk Co_3O_4 and STO, respectively, indicating direct electronic transitions inside these two materials. From the onset of the photoelectron quantum yield, as shown in the inset of Figure 4, a barrier height of Φ = 2.5 eV is identified. This energy barrier corresponds to the interband electronic transition from the VB of STO to the CB of Co_3O_4, i.e., Φ = VBO + $E_g^{Co_3O_4}$, as illustrated in the bottom inset of Figure 4. The deduced $E_g^{Co_3O_4}$ of 0.8 eV from IPE measurement matches well with our optically determined 0.74 eV, thus confirming both the position of the Co_3O_4 CB and conduction-band offsets (CBOs) between Co_3O_4 and STO.

We have also used core-level XPS to determine the extent of band bending on each side of the interface. If band bending occurs in the near-interface region, the core-level peaks for each atomic layer will slightly shift until a stable depletion region is established. In order to cancel the surface-charging effect during photoelectron ionization, we grow the Co_3O_4 thin film with different thicknesses on STO and align the measured XPS spectra with Sr 3d from the STO substrate,[43] as indicated in Figure 3b. The absence of an energy shift for Co 3p peaks with increasing film thickness from 1 to 3 nm suggests that there is

dx.doi.org/10.1021/am5036219 | ACS Appl. Mater. Interfaces 2014, 6, 14338−14344

no built-in electric field on the film side. This is in contrast to typical polar−nonpolar oxide heterostructures, e.g., $LaAlO_3$/STO[44,45] and $LaCrO_3$/STO,[43] the residual electrical potential of which is expected to be due to uncompensated polar discontinuity. To check the band bending on the substrate side, we focus on the Sr $3d_{5/2}$ peak because it exhibits a narrow peak with full-width at half-maximum (FWHM) near 1.0 eV; thus, any band bending of the magnitude comparable to the FWHM over the XPS probe depth will lead to measurable peak broadening for the Sr 3d spectrum. The measured Sr 3d FWHM values for all three heterojunctions are less than 0.1 eV larger than 1.0 eV of the bulk STO surface, which indicates that the STO substrate is also in a flat-band state.

Finally, a constructed experimental energy-level band-alignment diagram based on electrical and photoemission spectroscopy for epitaxial Co_3O_4/STO is illustrated in Figure 5. Because

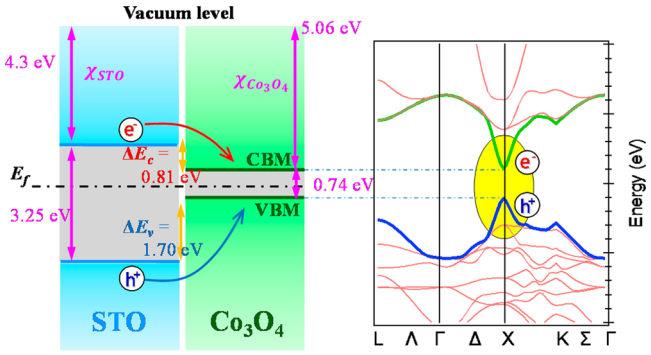

Figure 5. Constructed energy-level band alignment at the Co_3O_4/STO(001) heterojunction (left) and calculated band structure of Co_3O_4 (right). The complete overlap of both the VB and CB of the Co_3O_4 film with respect to the STO substrate indicates a type I heterojunction.

of the small value of the direct d−d gap for Co_3O_4 compared with the large indirect p−d gap for STO, the alignment of these two materials in energy space results in a large VB offset and a small CB offset at their interface, with the ratio of $\Delta E_v/\Delta E_c$ as ~2:1. As a consequence, the epitaxial Co_3O_4/STO has a straddling band alignment, forming a direct-gap type I heterojunction, which is similar to traditional semiconductor systems of GaN/InN and GaNAs/GaAs.[46,47] This type of band alignment will spatially confine both carriers of electrons and holes solely inside the thin Co_3O_4 layer with an electronic ground state belonging to the *X* minimum of the CB for Co_3O_4 (see the electronic band structure in the right panel of Figure 5). This behavior is unexpected because bulk Co_3O_4 is a typical p-type semiconductor, and it is thought that when combined with STO, a type II band alignment may form at the heterojunction, with carriers being spatially separated in real space, i.e., electrons being localized in the STO substrate and holes confined in the Co_3O_4 film. The formation of type I instead of type II band alignment is due to the intrinsic d−d interband excitation of Co_3O_4, which significantly narrows the fundamental band gap between the top of the VB and the bottom of the CB. Fortunately, for a Co_3O_4/STO heterojunction with a type I band alignment, we expect a much faster electron−hole recombination (due to the relatively large overlap of their wave functions) and a smaller radiative lifetime upon external photon or field excitation than with a type II heterojunction, where indirect transition is required between separated holes and electrons from both materials.

SUMMARY AND CONCLUSIONS

In summary, high-quality Co_3O_4/STO(001) heterojunctions with chemically abrupt interfaces have been prepared by pulsed laser deposition (PLD). VB and CB offsets have been determined by XPS to be 1.70 ± 0.08 and −0.81 ± 0.08 eV, respectively. Both XPS and IPE suggest a type I instead of type II band alignment for the heterojunction. The difference is ascribed to the intrinsic d−d interband excitation of Co_3O_4, which significantly narrows the fundamental band gap between the top of the VB and the bottom of the CB. No band bending is observed in either the film or substrate, suggesting a flat-band state. The obtained straddling band alignment with a flat CB or VB offset at the epitaxial Co_3O_4/STO heterojunction is very promising to be used in high-efficiency luminescence and optoelectronic devices.

METHODS

High-quality Co_3O_4 films were epitaxially grown on STO(001) substrates by PLD from a stoichiometric Co_3O_4 target. Laser ablation was performed at a repetition rate of 10 Hz and an energy density of 1.5 J/cm^2 with a 248 nm KrF excimer. Atomically flat TiO_2-terminated STO substrates were prepared as described previously.[48] Films were grown in 27 Pa oxygen, at a substrate temperature of 650 °C, and cooled to room temperature in 2.7 × 10^4 Pa O_2. Film thicknesses ranged from 1 to 200 nm and were determined by spectroscopic ellipsometry and cross-sectional scanning electron microscopy. Film growth was monitored by in situ RHEED, and the film thickness was measured by X-ray reflectivity. The crystal structure and epitaxial relationship were determined by high-resolution XRD using a PANalytical four-circle diffractometer in $2\theta-\omega$, rocking curve, φ scan, and RSM modes.

The electronic structure, band-edge alignment, energy offsets, and band bending were determined by XPS using a Thermo Scientific K-Alpha XPS instrument (certain commercial equipment, instruments, or materials are identified in this report in order to specify the experimental procedure adequately; such identification is not intended to imply recommendation or endorsement by the National Institute of Standards and Technology, nor is it intended to imply that the materials or equipment identified are necessarily the best available for the purpose), consisting of a hemispherical electron-energy analyzer and a monochromatic Al Kα_1 X-ray source. The absolute binding-energy scale was calibrated using the Au $4f_{7/2}$ core level at 84.00 ± 0.02 eV; thus, the Fermi-edge inflection point was at 0.00 ± 0.02 eV. For band-offset measurement, relatively thin epitaxial Co_3O_4/STO heterojunctions with thicknesses of a few nanometers were used because of the relatively smaller probe depth for soft XPS of ~45 Å. Sample charging during photoionization is a typical issue for semiconducting/insulating oxides; however, we had previously demonstrated that when properly tuned, the low-energy flood gun still allows high-energy resolution spectra to be obtained with essentially negligible line-shape distortion.[43]

The IPE measurement system is comprised of a 150 W broad-band xenon light source in conjunction with a grating monochromator. A regulated low-noise direct-current voltage supply provides the bias that is applied to the back gate of the test structure. An electrometer with subpicoampere precision records the photocurrent (I), while a monochromator scans the spectral range. The photoelectric quantum yield (Y) is defined as the ratio of the photocurrent and the flux (P) of the incident light. Further details of the measurement setup can be found elsewhere.[49] The measured device has a multilayer structure of Al_2O_3 (20 nm)/Co_3O_4 (50 nm)/STO (10 nm). A 20 nm atomic layer deposition Al_2O_3 film is used to reduce the leakage current and therefore to improve accurate data extraction.[50] Owing to its optical transparency and electrical conductivity, the top electrode is a large-area single-layer graphene grown by chemical vapor deposition and was transferred to the device surface.[41,42] The bottom electrode is 100

nm $SrRuO_3$, which is also grown by PLD. The whole device is epitaxially grown on an atomically flat STO(001) substrate.

■ ASSOCIATED CONTENT

Supporting Information

Additional XPS and peak fittings for the reference Co_3O_4 film and STO substrate. This material is available free of charge via the Internet at http://pubs.acs.org.

■ AUTHOR INFORMATION

Corresponding Authors

*E-mail: qiaol@ornl.gov.

*E-mail: biegalskim@ornl.gov.

Notes

The authors declare no competing financial interest.

■ ACKNOWLEDGMENTS

This research was conducted at the Center for Nanophase Materials Sciences and SHaRE User Facility, which are sponsored at Oak Ridge National Laboratory by the Scientific User Facilities Division, Office of Basic Energy Sciences, U.S. Department of Energy. The authors would like to thank the NIST Center for Nanoscale Science and Technology's Nanofab Facility for device fabrication support. H. Y. Xiao acknowledges the support of scientific research starting funding from University of Electronic Science and Technology of China (Grant No. Y02002010401085) and NSAF Joint Foundation of China (Grant No. U1330103). W. J. Weber was supported by the U.S. Department of Energy, Office of Basic Energy Sciences, Division of Materials Sciences and Engineering.

■ REFERENCES

(1) Kroemer, H. The Apparent Contact Potential of a Pseudo-abrupt p−n Junction. *RCA Rev.* **1956**, *17*, 515−521.

(2) Scanlon, D. O.; Dunnill, C. W.; Buckeridge, J.; Shevlin, S. A.; Logsdail, A. J.; Woodley, S. M.; Catlow, C. R. A.; Powell, M. J.; Palgrave, R. G.; Parkin, I. P.; Watson, G. W.; Keal, T. W.; Sherwood, P.; Walsh, A.; Sokol, A. A. Band Alignment of Rutile and Anatase TiO_2. *Nat. Mater.* **2013**, *12*, 798−801.

(3) Jin, S.; Tiefel, T. H.; McCormack, M.; Fastnacht, R. A.; Ramesh, R.; Chen, L. H. Thousandfold Change in Resistivity in Magnetoresistive La−Ca−Mn−O Films. *Science* **1994**, *264*, 413−415.

(4) Zheng, H.; Wang, J.; Lofland, S. E.; Ma, Z.; Mohaddes-Ardabili, L.; Zhao, T.; Salamanca-Riba, L.; Shinde, S. R.; Ogale, S. B.; Bai, F.; Viehland, D.; Jia, Y.; Schlom, D. G.; Wuttig, M.; Roytburd, A.; Ramesh, R. Multiferroic $BaTiO_3$−$CoFe_2O_4$ Nanostructures. *Science* **2004**, *303*, 661−663.

(5) Wang, J.; Neaton, J. B.; Zheng, H.; Nagarajan, V.; Ogale, S. B.; Liu, B.; Viehland, D.; Vaithyanathan, V.; Schlom, D. G.; Waghmare, U. V.; Spaldin, N. A.; Rabe, K. M.; Wuttig, M.; Ramesh, R. Epitaxial $BiFeO_3$ Multiferroic Thin Film Heterostructures. *Science* **2003**, *299*, 1719−1722.

(6) Ohtomo, A.; Hwang, H. Y. A High-mobility Electron Gas at the $LaAlO_3$/$SrTiO_3$ Heterointerface. *Nature* **2004**, *427*, 423−426.

(7) Chambers, S. A.; Engelhard, M. H.; Shutthanandan, V.; Zhu, Z.; Droubay, T. C.; Qiao, L.; Sushko, P. V.; Feng, T.; Lee, H. D.; Gustafsson, T.; Garfunkel, E.; Shah, A. B.; Zuo, J. M.; Ramasse, Q. M. Instability, Intermixing and Electronic Structure at the Epitaxial $LaAlO_3$/$SrTiO_3$(001) Heterojunction. *Surf. Sci. Rep.* **2010**, *65*, 317−352.

(8) Chen, Y. Z.; Bovet, N.; Trier, F.; Christensen, D. V.; Qu, F. M.; Andersen, N. H.; Kasama, T.; Zhang, W.; Giraud, R.; Dufouleur, J.; Jespersen, T. S.; Sun, J. R.; Smith, A.; Nygard, J.; Lu, L.; Buchner, B.; Shen, B. G.; Linderoth, S.; Pryds, N. A High-mobility Two-Dimensional Electron Gas at the Spinel/Perovskite Interface of γ-Al_2O_3/$SrTiO_3$. *Nat. Commun.* **2013**, *4*, 1371.

(9) Chuang, T. J.; Brundle, C. R.; Rice, D. W. Interpretation of X-ray Photoemission Spectra of Cobalt Oxides and Cobalt Oxide Surfaces. *Surf. Sci.* **1976**, *59*, 413−429.

(10) Ngamou, P. H. T.; Bahlawane, N. Influence of the Arrangement of the Octahedrally Coordinated Trivalent Cobalt Cations on the Electrical Charge Transport and Surface Reactivity. *Chem. Mater.* **2010**, *22*, 4158−4165.

(11) Gulino, A.; Fiorito, G.; Fragala, I. Deposition of Thin Films of Cobalt Oxides by MOCVD. *J. Mater. Chem.* **2003**, *13*, 861−865.

(12) Barreca, D.; Massignan, C.; Daolio, S.; Fabrizio, M.; Piccirillo, C.; Armelao, L.; Tondello, E. Composition and Microstructure of Cobalt Oxide Thin Films Obtained from a Novel Cobalt(II) Precursor by Chemical Vapor Deposition. *Chem. Mater.* **2001**, *13*, 588−593.

(13) Thota, S.; Kumar, A.; Kumar, J. Optical, Electrical and Magnetic Properties of Co_3O_4 Nanocrystallites Obtained by Thermal Decomposition of Sol−gel Derived Oxalates. *Mater. Sci. Eng., B* **2009**, *164*, 30−37.

(14) Kim, K. J.; Park, Y. R. Optical Investigation of Charge-Transfer Transitions in Spinel Co_3O_4. *Solid State Commun.* **2003**, *127*, 25−28.

(15) Donders, M. E.; Knoops, H. C. M.; van de Sanden, M. C. M.; Kessels, W. M. M.; Notten, P. H. L. Remote Plasma Atomic Layer Deposition of Co_3O_4 Thin Films. *J. Electrochem. Soc. 158*, G92−G96.

(16) Kawasaki, M.; Takahashi, K.; Maeda, T.; Tsuchiya, R.; Shinohara, M.; Ishiyama, O.; Yonezawa, T.; Yoshimoto, M.; Koinuma, H. Atomic Control of the $SrTiO_3$ Crystal-Surface. *Science* **1994**, *266*, 1540−1542.

(17) Koster, G.; Kropman, B. L.; Rijnders, G.; Blank, D. H. A.; Rogalla, H. Quasi-Ideal Strontium Titanate Crystal Surfaces Through Formation of Strontium Hydroxide. *Appl. Phys. Lett.* **1998**, *73*, 2920−2922.

(18) Schwartz, G. P.; Hybertsen, M. S.; Bevk, J.; Nuzzo, R. G.; Mannaerts, J. P.; Gualtieri, G. J. Core-Level Photoemission Measurements of Valence-band Offsets in Highly Strained Heterojunctions—Si−Ge System. *Phys. Rev. B* **1989**, *39*, 1235−1241.

(19) Martin, G.; Botchkarev, A.; Rockett, A.; Morkoc, H. Valence-Band Discontinuities of Wurtzite GaN, AlN, and InN Heterojunctions Measured by X-ray Photoemission Spectroscopy. *Appl. Phys. Lett.* **1996**, *68*, 2541−2543.

(20) Narayan, J.; Larson, B. C. Domain Epitaxy: A Unified Paradigm for Thin Film Growth. *J. Appl. Phys.* **2003**, *93*, 278−285.

(21) Qiao, L.; Xiao, H. Y.; Weber, W. J.; Biegalski, M. D. Coexistence of Epitaxial Lattice Rotation and Twinning Tilt Induced by Surface Symmetry Mismatch. *Appl. Phys. Lett.* **2014**, *104*, 221602.

(22) Qiao, L.; Bi, X. F. Origin of Compressive Strain and Phase Transition Characteristics of Thin $BaTiO_3$ Film Grown on $LaNiO_3$/Si Substrate. *Phys. Status Solidi A* **2010**, *207*, 2511−2516.

(23) Matthews, J. W.; Blakeslee, A. E. Defects in Epitaxial Multilayers. 1. Misfit Dislocations. *J. Cryst. Growth* **1974**, *27*, 118−125.

(24) Qiao, L.; Droubay, T. C.; Kaspar, T. C.; Sushko, P. V.; Chambers, S. A. Cation Mixing, Band Offsets and Electric Fields at $LaAlO_3$/$SrTiO_3$(001) Heterojunctions with Variable La:Al Atom Ratio. *Surf. Sci.* **2011**, *605*, 1381−1387.

(25) Qiao, L.; Droubay, T. C.; Shutthanandan, V.; Zhu, Z.; Sushko, P. V.; Chambers, S. A. Thermodynamic Instability at the Stoichiometric $LaAlO_3$/$SrTiO_3$(001) interface. *J. Phys.: Condens. Matter* **2010**, *22*, 312201.

(26) Kraut, E. A.; Grant, R. W.; Waldrop, J. R.; Kowalczyk, S. P. Precise Determination of the Valence-band Edge in X-ray Photoemission Spectra—Application to Measurement of Semiconductor Interface Potentials. *Phys. Rev. Lett.* **1980**, *44*, 1620−1623.

(27) Kraut, E. A.; Grant, R. W.; Waldrop, J. R.; Kowalczyk, S. P. Semiconductor Core-level to Valence-band Maximum Binding-energy Differences—Precise Determination by X-ray Photoelectron Spectroscopy. *Phys. Rev. B* **1983**, *28*, 1965−1977.

(28) Chambers, S. A.; Liang, Y.; Yu, Z.; Droopad, R.; Ramdani, J.; Eisenbeiser, K. Band Discontinuities at Epitaxial $SrTiO_3$/Si(001) Heterojunctions. *Appl. Phys. Lett.* **2000**, *77*, 1662−1664.

(29) Chambers, S. A.; Droubay, T.; Kaspar, T. C.; Gutowski, M. Experimental Determination of Valence Band Maxima for $SrTiO_3$, TiO_2, and SrO and the Associated Valence Band Offsets with Si(001). *J. Vac. Sci. Technol. B* **2004**, *22*, 2205−2215.
(30) Shinde, V. R.; Mahadik, S. B.; Gujar, T. P.; Lokhande, C. D. Supercapacitive Cobalt Oxide (Co_3O_4) Thin Films by Spray Pyrolysis. *Appl. Surf. Sci.* **2006**, *252*, 7487−7492.
(31) Chen, J.; Wu, X. F.; Selloni, A. Electronic Structure and Bonding Properties of Cobalt Oxide in the Spinel Structure. *Phys. Rev. B* **2011**, *83*, 245204.
(32) Qiao, L.; Xiao, H.; Meyer, H.; Sun, J.; Rouleau, C. M.; Puretzky, A.; Geohegan, D.; Ivanov, I. N.; Yoon, M.; Weber, W. J.; Biegalski, M. Nature of the Band Gap and Origin of the Electro-/photoactivity of Co_3O_4. *J. Mater. Chem. C* **2013**, *1*, 4628−4633.
(33) van Benthem, K.; Elsasser, C.; French, R. H. Bulk Electronic Structure of $SrTiO_3$: Experiment and Theory. *J. Appl. Phys.* **2001**, *90*, 6156−6164.
(34) Piskunov, S.; Heifets, E.; Eglitis, R. I.; Borstel, G. Bulk Properties and Electronic Structure of $SrTiO_3$, $BaTiO_3$, $PbTiO_3$ Perovskites: an Ab Initio HF/DFT Study. *Comput. Mater. Sci.* **2004**, *29*, 165−178.
(35) Anderson, R. L. Germanium−gallium Arsenide Heterojunctions. *IBM J. Res. Dev.* **1960**, *4*, 283−287.
(36) Henrich, V. E.; Dresselhaus, G.; Zeiger, H. J. Surface Defects and Electronic-Structure of $SrTiO_3$ Surfaces. *Phys. Rev. B* **1978**, *17*, 4908−4921.
(37) Miura, A.; Uraoka, Y.; Fuyuki, T.; Yoshii, S.; Yamashita, I. Floating Nanodot Gate Memory Fabrication with Biomineralized Nanodot as Charge Storage Node. *J. Appl. Phys.* **2008**, *103*, 10.
(38) Keng, P. Y.; Kim, B. Y.; Shim, I. B.; Sahoo, R.; Veneman, P. E.; Armstrong, N. R.; Yoo, H.; Pemberton, J. E.; Bull, M. M.; Griebel, J. J.; Ratcliff, E. L.; Nebesny, K. G.; Pyun, J. Colloidal Polymerization of Polymer-Coated Ferromagnetic Nanoparticles into Cobalt Oxide Nanowires. *ACS Nano* **2009**, *3*, 3143−3157.
(39) Jugnet, Y.; Duc, T. M. Structure Electronic of Oxides of Cobalt CoO and Co_3O_4. *J. Phys. Chem. Solids* **1979**, *40*, 29−37.
(40) Grellner, F.; Klingenberg, B.; Borgmann, D.; Wedler, G. Interaction of H_2O with $C_O(1120)$—A Photoelectron Spectroscopic Study. *Surf. Sci.* **1994**, *312*, 143−150.
(41) Xu, K.; Zeng, C.; Zhang, Q.; Yan, R.; Ye, P.; Wang, K.; Seabaugh, A. C.; Xing, H. G.; Suehle, J. S.; Richter, C. A.; Gundlach, D. J.; Nguyen, N. V. Direct Measurement of Dirac Point Energy at the Graphene/Oxide Interface. *Nano Lett.* **2013**, *13*, 131−136.
(42) Rusen, Y.; Zhang, Q.; Kirillov, O. A.; Li, W.; Basham, J.; Boosalis, A.; Liang, X.; Jena, D.; Richter, C. A.; Seabaugh, A. C.; Gundlach, D. J.; Xing, H. G.; Nguyen, N. V. Graphene as Transparent Electrode for Direct Observation of Hole Photoemission from Silicon to Oxide. *Appl. Phys. Lett.* **2013**, *102*, 123106.
(43) Chambers, S. A.; Qiao, L.; Droubay, T. C.; Kaspar, T. C.; Arey, B. W.; Sushko, P. V. Band Alignment, Built-In Potential, and the Absence of Conductivity at the $LaCrO_3/SrTiO_3(001)$ Heterojunction. *Phys. Rev. Lett.* **2011**, *107*, 206802.
(44) Singh-Bhalla, G.; Bell, C.; Ravichandran, J.; Siemons, W.; Hikita, Y.; Salahuddin, S.; Hebard, A. F.; Hwang, H. Y.; Ramesh, R. Built-in and Induced Polarization Across $LaAlO_3/SrTiO_3$ heterojunctions. *Nat. Phys.* **2011**, *7*, 80−86.
(45) Liang, H. X.; Cheng, L.; Zhai, X. F.; Pan, N.; Guo, H. L.; Zhao, J.; Zhang, H.; Li, L.; Zhang, X. Q.; Wang, X. P.; Zeng, C. G.; Zhang, Z. Y.; Hou, J. G. Giant Photovoltaic Effects Driven by Residual Polar Field within Unit-Cell-Scale $LaAlO_3$ Films on $SrTiO_3$. *Sci. Rep.* **2013**, *3*, 1975.
(46) King, P. D. C.; Veal, T. D.; Kendrick, C. E.; Bailey, L. R.; Durbin, S. M.; McConville, C. F. InN/GaN Valence Band Offset: High-resolution X-ray Photoemission Spectroscopy Measurements. *Phys. Rev. B* **2008**, *78*, 033308.
(47) Buyanova, I. A.; Pozina, G.; Hai, P. N.; Chen, W. M.; Xin, H. P.; Tu, C. W.; Type, I. Band Alignment in the GaN_xAs_{1-x}/GaAs Quantum Wells. *Phys. Rev. B* **2001**, *63*, 033303.
(48) Qiao, L.; Droubay, T. C.; Varga, T.; Bowden, M. E.; Shutthanandan, V.; Zhu, Z.; Kaspar, T. C.; Chambers, S. A. Epitaxial Growth, Structure, and Intermixing at the $LaAlO_3/SrTiO_3$ Interface As the Film Stoichiometry is Varied. *Phys. Rev. B* **2011**, *83*, 085408.
(49) Nguyen, N. V.; Kirillov, O. A.; Suehle, J. S. Band Alignment of Metal-oxide-semiconductor Structure by Internal Photoemission Spectroscopy and Spectroscopic Ellipsometry. *Thin Solid Films* **2011**, *519*, 2811−2816.
(50) Zhang, Q.; Zhou, G.; Xing, H. G.; Seabaugh, A. C.; Xu, K.; Sio, H.; Kirillov, O. A.; Richter, C. A.; Nguyen, N. V. Tunnel Field-effect Transistor Heterojunction Band Alignment by Internal Photoemission Spectroscopy. *Appl. Phys. Lett.* **2012**, *100*, 102104.